Residual stress effects on the propagation of fatigue cracks in the weld of a CA6NM stainless steel

Alexandre Trudel[1,*], Myriam Brochu[1], Martin Lévesque[1]

[1] Department of Mechanical Engineering, École Polytechnique de Montréal, Montreal, Canada
* Corresponding author: alexandre.trudel@polymtl.ca

Abstract   The fatigue crack growth behavior in an automatic flux core arc weld was investigated for stainless steel alloy CA6NM. As-welded and heat treated compact tension specimens were prepared with the crack propagation plane perpendicular to the weld. Constant stress intensity factor range tests were performed at a load ratio R = 0.1 to reveal intra-specimen fatigue crack growth rate variations and differences between the fatigue crack growth behavior of as-welded and heat treated specimens. Comparing the fatigue crack growth rate of as-welded and heat treated specimens revealed that the crack propagates at a faster rate in the as-welded specimens where indications point to the existence of tensile residual stresses acting on the crack tip by inhibiting crack closure. As for the heat treated specimens, when the crack is in the base metal, the fatigue crack growth rate decreases accompanied by an increase in crack closure levels. Tensile residual stresses that may have remained after the post-weld heat treatment and their subsequent relaxation with crack growth could explain this behavior.

Keywords   Welding, Stainless Steel, Fatigue Crack Growth, Residual Stresses, Crack Closure

1. Introduction

Cast martensitic stainless steel alloy CA6NM has been used to manufacture hydraulic turbine runners for many decades. Its high strength, weldability and resistance to corrosion and cavitation damage make it a prime candidate for this application. Turbine runners are manufactured by welding cast blades to a cast core using a matching filler metal such as 410NiMo. During service, the cyclic loads acting on the runners can lead to fatigue failures [1]. A damage tolerance approach for the stress analysis of turbine runners can be an efficient strategy to account for the discontinuities, such as casting and welding defects as well as partial penetration weld joint designs, found in these components. A good knowledge of material resistance to fatigue crack growth is therefore needed.

During welding, residual stresses develop and are believed to have a significant influence on the fatigue crack growth behavior of CA6NM welds. Weld-induced residual stresses arise from the elastic interactions between the constraining base metal and the weld metal shrinkage upon solidification and cooling. In stainless steel CA6NM, the volumetric expansion resulting from the austenite to martensite transformation, in conjunction with the low transformation temperature, contributes to the buildup of residual stresses during the welding process [2]. Previous studies have shown that significant tensile and compressive residual stresses can be found in as-welded CA6NM welds [2, 3]. These studies have also shown that post-weld heat treatment (tempering) can reduce the residual stress level. Thibault and al. obtained a 75 percent reduction of the maximum tensile residual stress measured in a five beads V-preparation weld (534 MPa to 136 MPa) [2]. Moisan and al. also showed that the maximum average tensile residual stress in a multi-pass T-joint was reduced after post-weld heat treatment by an amount of 73 percent (204 MPa to 56 MPa) [3].

A fatigue crack growing in a weld can be under the influence of tensile or compressive residual stresses, depending on the geometry of the joint and the position of the crack tip. Under tensile residual stresses, the crack tip is submitted to higher maximum and minimum loads resulting in a higher effective load ratio. This can also affect the effective stress intensity factor range as it can prevent closure, often resulting in higher fatigue crack growth rates (FCGR) [4-6]. On the other hand, compressive residual stresses can accentuate crack closure and be beneficial if they reduce the effective stress intensity factor range and thus the fatigue crack growth rate [5].

The main objective of this study was to characterize the effect of residual stresses on the fatigue crack growth behavior of a flux-cored arc weld consisting of alloy CA6NM and filler metal 410NiMo. Intra-specimen fatigue crack growth rate variations between the filler metal (FM), heat affected zone (HAZ) and base metal (BM), as well as the effect of post-weld heat treatment on fatigue crack growth behavior were studied. Microhardness profiles and metallographic observations were realized on as-welded (AW) and heat treated (HT) specimens encompassing the three zones (FM, HAZ and BM) in order to position the fusion line and determine the width of the heat affected zone. Fatigue crack growth tests were carried out at constant stress intensity factor ranges in order to highlight the effect of residual stresses on the fatigue crack growth behavior. The results are discussed based on the effect of the residual stresses as well as crack closure.

2. Experimental procedure

2.1. Materials

The materials used in this study are base metal martensitic stainless steel alloy CA6NM, and the matching filler metal 410NiMo. The chemical composition and mechanical properties of the CA6NM alloy used are given in Table 1 and Table 2, respectively. Using a fully automated flux-cored arc welding (FCAW) process, 40 mm of weld was built up at the surface of a 50 mm thick CA6NM plate. The welding parameters are given in Table 3. The welded plate was cut in two parts, one of which underwent a post-weld heat treatment at 600°C for two hours. Specimens were prepared from both plates for microhardness measurements and fatigue testing.

Table 1. Chemical composition of base metal CA6NM (weight %) [7]

Material	C	Mn	Si	S	P	Cr	Ni	Mo
CA6NM	0.02	0.66	0.59	0.008	0.031	13.04	4.07	0.53

Table 2. Mechanical properties of base metal CA6NM [7]

Yield strength	Tensile strength	Young's Modulus	Elongation	Reduction Area
763 MPa	837 MPa	206 GPa	27.0 %	58.8 %

Table 3. Welding parameters

Process	Shielding gas	Wire diameter	Voltage	Current	Speed	Heat input
FCAW	75% Ar, 25% CO_2	1.6 mm	27.5 V	260 A	5 mm/s	1.4 kJ/mm

2.2 Microhardness measurements and metallographic observations

As-welded (AW) and heat treated (HT) specimens encompassing the three zones (FM, HAZ and BM) were sampled for microhardness measurements and metallographic observations. A rough polish was performed with abrasive paper of grit sizes ranging from 240 to 600, followed by a final polish using polycrystalline diamond suspension of sizes 6 μm, 3 μm and 1 μm. Vickers microhardness profiles were taken across the as-welded and heat treated specimens using a force of 100 gf and a dwell time of 15 seconds. The indentation spacing was 100 μm and measurements were taken on a length of 12 mm starting in the filler metal up to the unaffected base metal. A modified Fry's reagent was used to chemically etch the specimens and metallographic observations were realized to position the fusion line.

2.3. Fatigue testing

Compact tension (CT) specimens having a width of 50.8 mm and a thickness of 12.7 mm were machined from heat treated and as-welded plates in accordance with ASTM E647 [8]. The notches were aligned perpendicularly to the welding direction to allow for the crack to grow through each zone of the joint (FM, HAZ and BM). As seen in Fig. 1, the crack tip was positioned in the filler metal at 7 mm from the fusion line (FL). Constant stress intensity factor range tests in river water environment were performed at a constant load ratio R = 0.1 and at a frequency of 20 Hz using a 100 kN MTS servo-hydraulic machine. As-welded and heat treated specimens were tested at stress intensity factor ranges of 8 MPa·m^{½} and 20 MPa·m^{½}. The crack length was continuously monitored using the compliance method with a crack mouth clip gauge. The load and crack opening displacement (COD) were recorded for every cycle and used to determine the closure loads. The closure stress intensity factor (K_{cl}) was defined for a compliance offset of 2 percent [8]. The effective stress intensity factor range (ΔK_{eff}) was calculated by the difference between the maximum applied stress intensity factor (K_{max}) and the closure stress intensity factor (K_{cl}).
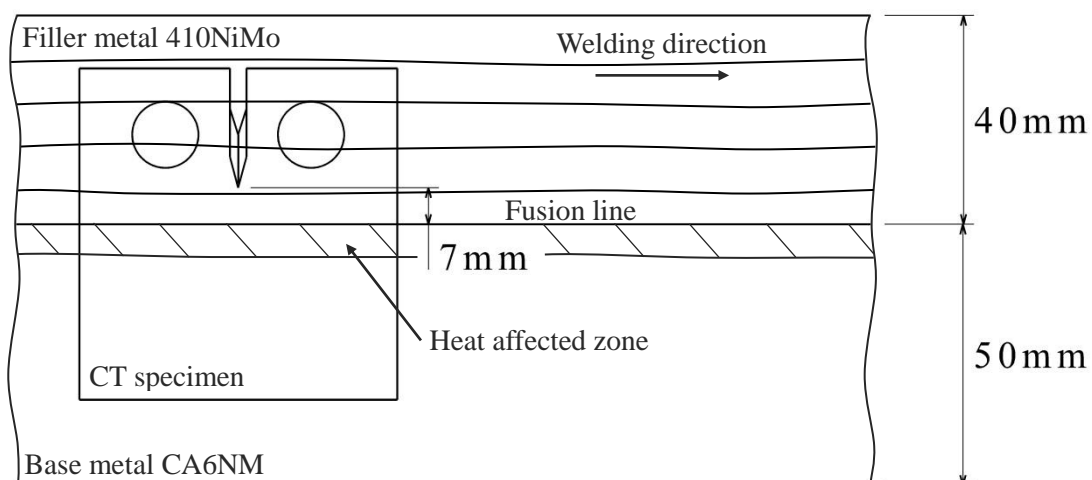

Figure 1. Compact tension specimen sampling layout. Starter notch aligned perpendicularly to the welding direction. Crack tip positioned at 7 mm from the fusion line in the FM.

3. Results

3.1. Microhardness measurements and metallographic observations

The microhardness profiles of the as-welded and heat treated specimens are shown in Fig. 2a and b, respectively. Metallographic observations were realized to identify the position of the fusion line as shown in Fig. 3 for an as-welded joint. The microstructure of the heat treated joint is visually similar and has been omitted. The heat affected zone extends from the fusion line to the microhardness plateau characterizing the base metal, as indicated in Fig. 2. The shape of the microhardness profile is similar for both specimens. The microhardness has its highest value in the filler metal and decreases from the fusion line down to characteristic values of the base metal. The heat affected zone extends up to about 5 mm from the fusion line. The main difference between the two profiles is the microhardness of the filler metal, which is 360 HV on average in the as-welded condition and 325 HV following the tempering heat treatment. These results are in good agreement with what was measured by Thibault and al. from a FCAW CA6NM joint using filler metal 410NiMo [9].
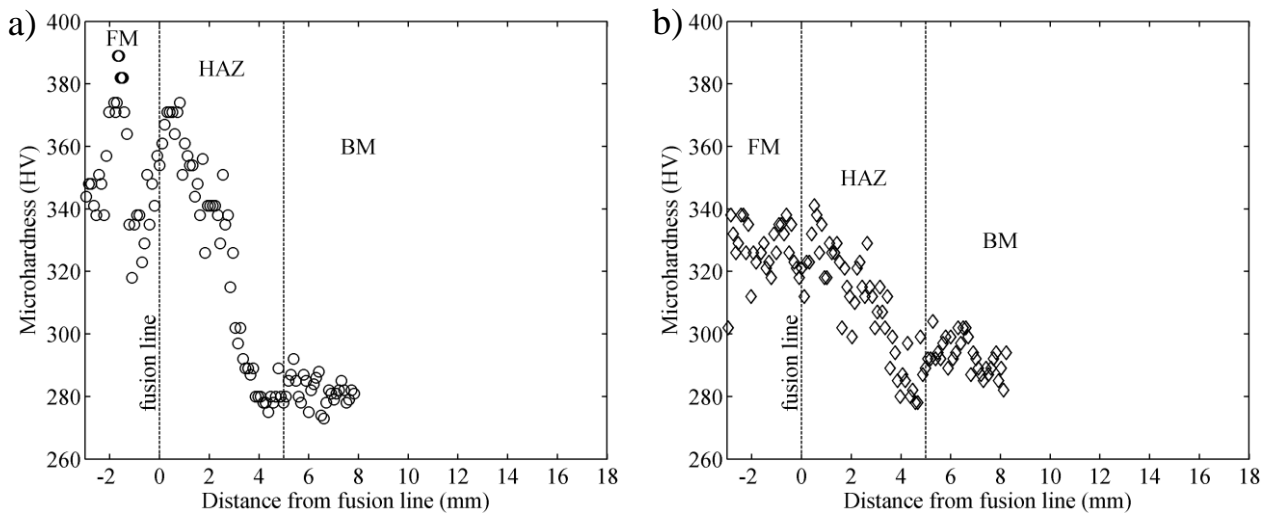

Figure 2. Microhardness profiles a) As-welded specimen b) Heat treated specimen, 2 hours at 600°C
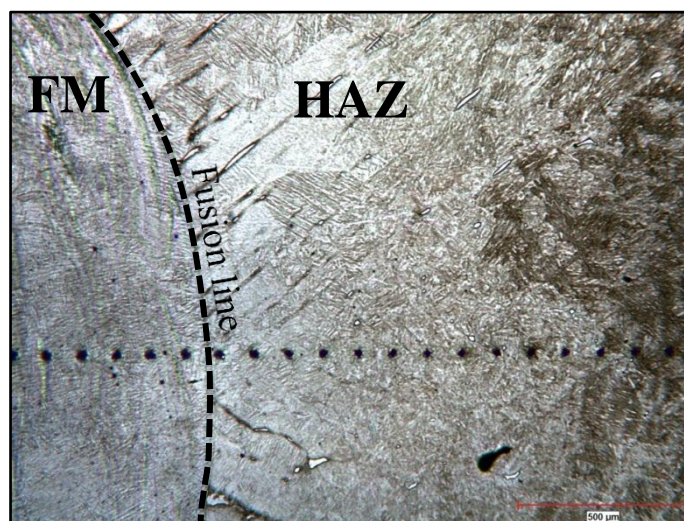

Figure 3. As-welded joint microstructure near the fusion line revealed by etching (50X).

3.2 Fatigue tests

Fig. 4 shows the results of the fatigue tests for as-welded and heat treated specimens at $\Delta K = 8$ MPa·m$^{1/2}$ and $\Delta K = 20$ MPa·m$^{1/2}$. Table 4 shows the mean fatigue crack growth rate in the three zones (FM, HAZ and BM) of as-welded and heat treated specimens. When comparing a given zone at a given stress intensity factor range, the fatigue crack growth rate is always lower in the heat treated specimens than in the as-welded specimens, suggesting that the post-weld heat treatment improves the fatigue crack growth resistance. Pukasiewicz et al. found a similar behavior where the fatigue crack growth rate in the fusion zone of an as-welded CA6NM welded joint was considerably lowered after post-weld heat treatment [10]. In as-welded specimens, the fatigue crack growth rate decreases regularly from the filler metal and into the heat affected zone, before stabilizing in the base metal for both stress intensity factor ranges. These intra-specimen variations are believed to be attributed to microstructural effects and are the subject of an ongoing research. The gradual decrease of the fatigue crack growth rate is not observed in the heat treated specimen. At $\Delta K = 8$ MPa·m$^{1/2}$, the fatigue crack growth rate remains fairly constant up to 9 mm from the fusion line (4 mm into the base metal), then decreases by approximately 50 percent and stabilizes at 13 mm from the fusion line. The same behavior, though less pronounced, is also observed at $\Delta K = 20$ MPa·m$^{1/2}$, where the fatigue crack growth rate decreases by approximately 20 percent.
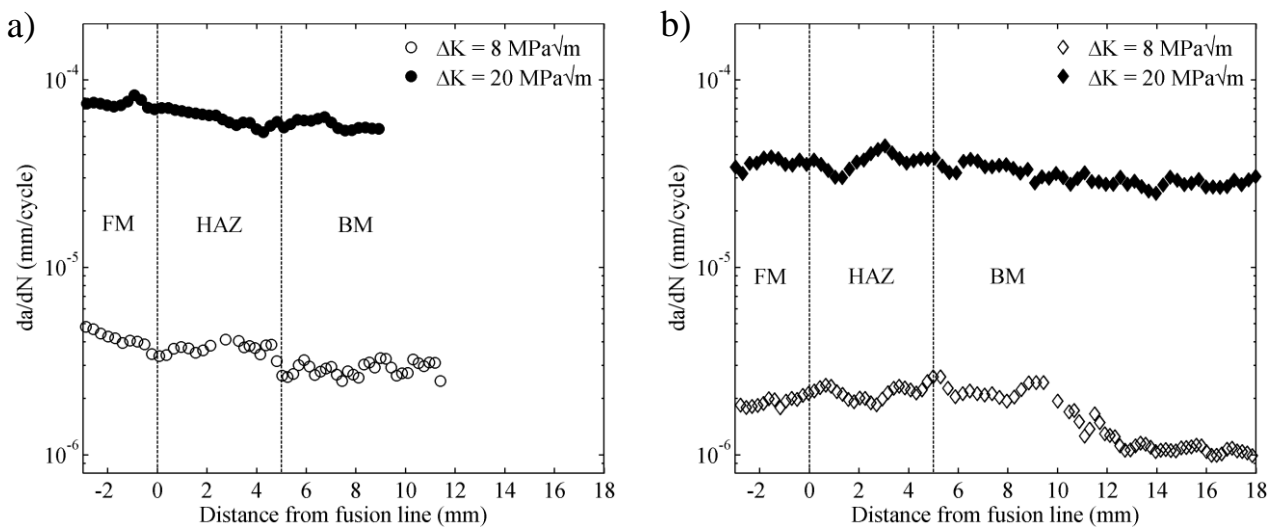

Figure 4. Constant ΔK test results a) As-welded specimens b) Heat treated specimens

Table 4. Mean FCGR in the FM, HAZ and BM of as-welded and heat treated specimens

ΔK (MPa·m$^{1/2}$)	Fatigue crack growth rate (mm/cycle)						
	As-welded specimens			Heat treated specimens			
	FM	HAZ	BM	FM	HAZ	BM	
						Up to 9 mm from FL	After 13 mm from FL
8	$4.2 \cdot 10^{-6}$	$3.7 \cdot 10^{-6}$	$2.9 \cdot 10^{-6}$	$1.9 \cdot 10^{-6}$	$2.1 \cdot 10^{-6}$	$2.2 \cdot 10^{-6}$	$1.1 \cdot 10^{-6}$
20	$7.5 \cdot 10^{-5}$	$6.3 \cdot 10^{-5}$	$5.8 \cdot 10^{-5}$	$3.6 \cdot 10^{-5}$	$3.7 \cdot 10^{-5}$	$3.5 \cdot 10^{-5}$	$2.8 \cdot 10^{-5}$

4. Discussion

This section presents an analysis of the constant stress intensity factor range tests results. The higher fatigue crack growth rates found in the as-welded specimens are discussed in terms of tensile residual stresses causing the opening of the crack. The fatigue crack growth rate variations observed in the heat treated specimens are discussed in terms of residual stress relaxation and crack closure. Fig. 5 shows the base metal fatigue crack growth curves obtained at load ratios R = 0.1 and R = 0.7 [1], along with the mean fatigue crack growth rate obtained in the base metal from the constant stress intensity factor range test results (Table 4). The mean fatigue crack growth rate in the base metal of the heat treated specimens was calculated from the stabilized data starting at 13 mm from the fusion line. For the heat treated specimens, a good agreement is found between the R = 0.1 base metal fatigue crack growth curve and the fatigue test results, for both stress intensity factor ranges. These results, along with the intra-specimen fatigue crack growth rate variations noted in the last section (Fig. 4b), are discussed further in terms of residual stress relaxation and crack closure. Furthermore, the fatigue crack growth rates in the as-welded specimens at $\Delta K = 8$ MPa·m$^{\frac{1}{2}}$ (empty circles) and $\Delta K = 20$ MPa·m$^{\frac{1}{2}}$ (filled circles) correlate well with the R = 0.7 base metal baseline. Several indications suggesting the presence of tensile residual stresses responsible for the higher effective load ratio seen by the as-welded specimens are discussed next.

4.1. Fatigue crack growth behavior of as-welded specimens

The typical load-compliance offset curve for as-welded specimens is shown in Fig. 6a. For both stress intensity factor ranges and at all crack lengths, the specimen's response does not deviate from the fully-open crack compliance. This indicates that the crack remains fully-open and that the effective stress intensity factor range is equal to the applied stress intensity factor range. This corresponds to an effective stress intensity factor range ratio ($U = \Delta K_{eff}/\Delta K$) equal to unity in Fig. 6b (circles). It is well known that, for ductile materials free of residual stresses, plasticity-induced crack closure plays a significant role in reducing the effective stress intensity factor range [11].
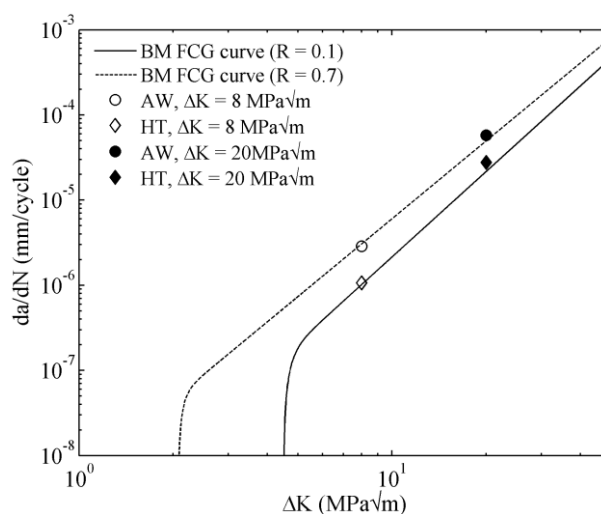

Figure 5. Comparison between the mean FCGR in the BM obtained from the constant ΔK tests and the BM fatigue crack growth curve in the Paris regime at load ratios R = 0.1 and R = 0.7 [1]
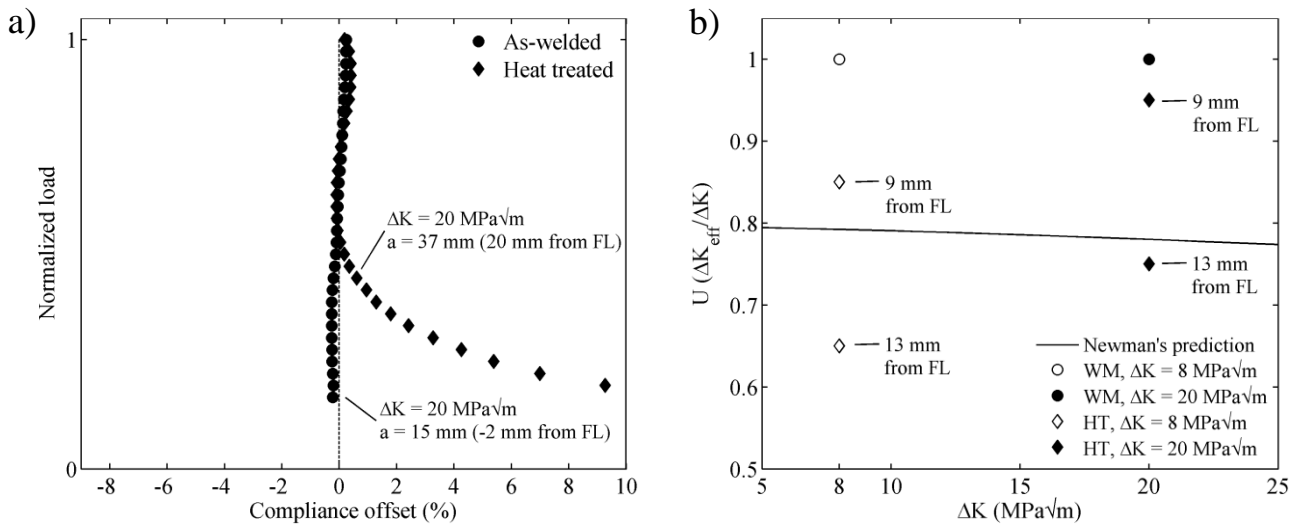
Figure 6. a) Typical load-compliance offset curves for as-welded and heat treated specimens. b) Comparison between experimental values of U and Newman's prediction

The solid line in Fig. 6b was calculated using Newman's plasticity-induced closure stress equation [12, 13] and represents an upper bound of the effective stress intensity factor range ratio. Experimental data above this upper bound indicate the existence of a crack opening mechanism. Tensile residual stresses are believed to act as such a mechanism in the as-welded specimens, since tensile residual stresses are typically found in CA6NM welds.

To further assess the presence of tensile residual stresses, an as-welded compact tension specimen with a crack length of 20 mm was incrementally loaded from 500 N to -12000 N and the crack opening displacement was recorded (Fig. 7). A closure load of -1000 N was found with a 2 percent compliance offset criterion. The existence of a negative closure load is another strong indication that tensile residual stresses are acting on the crack by preventing it to close at positive loads. A similar behavior has been observed in the welds of three different kinds of steels where tensile residual stresses caused the crack to remain fully open at a load ratio R = 0, resulting in higher fatigue crack growth rates than that of the base metal [5].
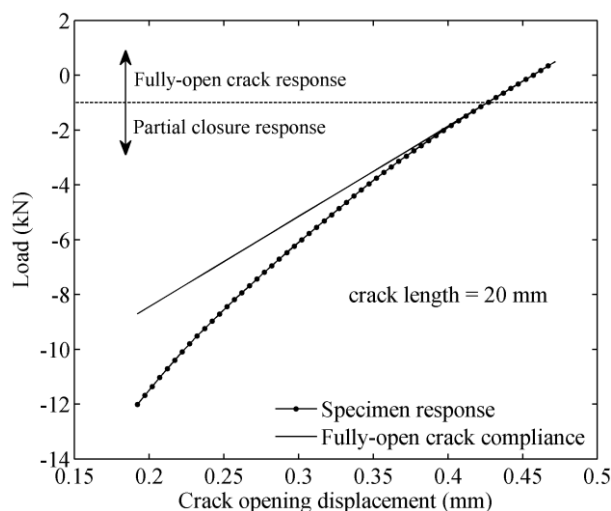

Figure 7. As-welded specimen load-COD curve from a single compression excursion (a = 20 mm)

4.2. Fatigue crack growth behavior of heat treated specimens

The crack closure behavior of the heat treated specimens is different. Crack closure was observed at both stress intensity factor ranges and for all crack lengths and the typical load-compliance offset curve is shown in Fig. 6a. Fig. 6b shows the effective stress intensity factor range ratio for the heat treated specimens when the crack is at 9 mm from the fusion line and at 13 mm from the fusion line. As a first observation, crack closure is more important at $\Delta K = 8$ MPa·m$^{\frac{1}{2}}$ for equal crack lengths. This is expected since crack closure is more pronounced for low stress intensity factor ranges [14]. Furthermore, up to 9 mm from the fusion line, the effective stress intensity factor range ratio remains above Newman's theoretical upper bound for both stress intensity factor ranges. This is an indication that tensile residual stresses may have remained after post-weld heat treatment, partially inhibiting crack closure. These results are consistent with previous studies that showed that the post-weld heat treatment may not completely eliminate the residual stresses in CA6NM welds [2, 3]. On the other hand, the effective stress intensity factor range ratio of the crack at 13 mm from the fusion line is below the upper bound predicted by Newman for plasticity-induced crack closure for both stress intensity factor ranges. This is an indication that tensile residual stresses at the crack tip may have relaxed with crack growth and that crack closure is not inhibited. Tensile residual stresses are known to redistribute and eventually relax following the growth of a fatigue crack [15]. After complete relaxation of the tensile residual stresses, common closure mechanisms such as plasticity-induced, roughness-induced and oxide-induced crack closure become fully active and the global closure level is increased.

The evolution of the measured effective stress intensity factor range ratio against the crack length is shown in Fig. 8 (triangles). Crack closure is rather constant up to 9 mm from the fusion line, than it increases as the crack grows and eventually stabilizes. A good correlation is observed between the profiles of the fatigue crack growth rate (circles) and the effective stress intensity factor range ratio (triangles). This shows that the fatigue crack growth behavior of the heat treated specimens is directly affected by the variation of crack closure.
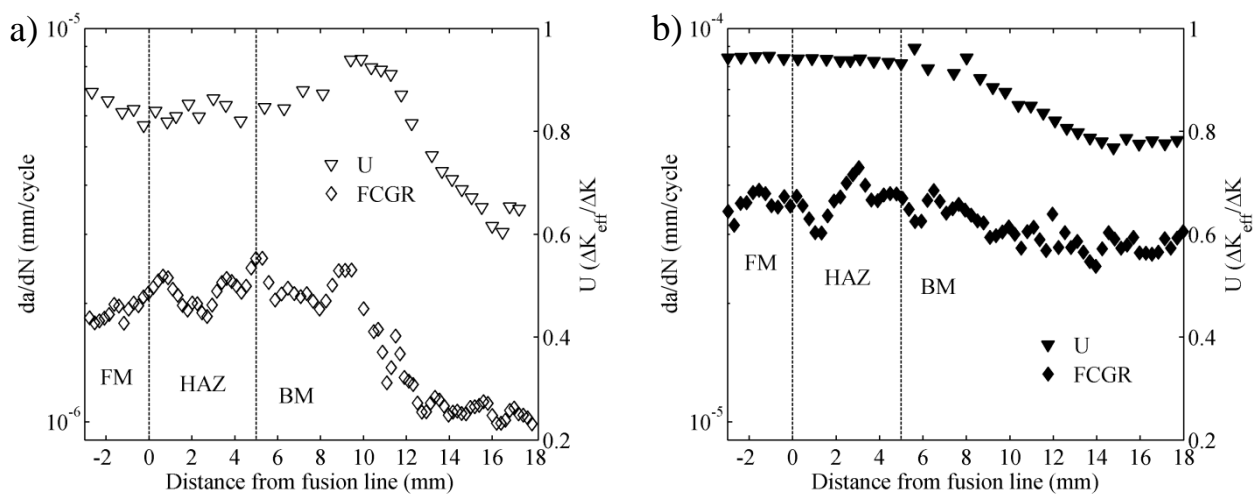

Figure 8. Relationship between U and the FCGR against the crack length for heat treated specimens
a) $\Delta K = 8$ MPa·m$^{\frac{1}{2}}$ b) $\Delta K = 20$ MPa·m$^{\frac{1}{2}}$

5. Conclusion

The main objective of this study was to investigate the effect of residual stresses on the fatigue crack growth behavior of a stainless steel alloy CA6NM welded joint. From the results, the following conclusions can be drawn.

In as-welded specimens, many clues point to the fact that tensile residual stresses are present at the crack tip and are having an effect on the fatigue crack growth behavior. This hypothesis is supported by: (1) A higher effective load ratio indicated by the agreement between the mean R = 0.1 experimental base metal fatigue crack growth rate and the R = 0.7 base metal fatigue crack growth curve. (2) An effective stress intensity factor range ratio equal to unity for all crack lengths meaning that a crack opening mechanism is present. (3) A negative closure load on an as-welded specimen at a crack length of 20 mm.

It is also believed that some tensile residual stresses remain after post-weld heat treatment, as evidenced by the effective stress intensity factor range ratio being superior to Newman's prediction for plasticity-induced crack closure. In addition, an increase in crack closure when the crack is in the base metal points to the fact that the tensile residual stresses were relaxed with crack growth and that closure mechanisms become fully active.

This study showed that tensile residual stresses, which are strongly believed to be present in the as-welded specimens, caused the crack to remain fully open, this having a detrimental effect on the fatigue crack growth resistance of CA6NM welds. Moreover, the fatigue crack growth resistance was found to be improved in the heat treated specimens compared to the as-welded specimens. This is attributed to the residual stresses relaxation after tempering and with crack growth, allowing closure mechanisms to become active and reducing the fatigue crack growth rates. This shows the importance of a good residual stress level control through post-weld heat treatment.

References
[1]   M. Sabourin, D. Thibault, D. A. Bouffard, and M. Levesque, "New parameters influencing hydraulic runner lifetime," presented at the 25th IAHR Symposium on Hydraulic Machinery and Systems, Timisoara, Romania, 2010.

[2]   D. Thibault, P. Bocher, M. Thomas, M. Gharghouri, and M. Côté, "Residual stress characterization in low transformation temperature 13%Cr–4%Ni stainless steel weld by neutron diffraction and the contour method," *Mat Sci Eng A-Struct,* vol. 527, pp. 6205-6210, 2010.

[3]   É. Moisan, M. Sabourin, M. Bernard, and T. Bui-Quoc, "Residual stress measurements in hydraulic turbine welded joints," presented at the IAHR 23rd Symposium on Hydraulic Machinery and Systems, Yokohama, Japan, 2006.

[4]   Y. B. Lee, C. S. Chung, Y. K. Park, and H. K. Kim, "Effects of redistributing residual stress on the fatigue behavior of SS330 weldment," *Int J Fatigue,* vol. 20, pp. 565-573, 1998.

[5]   A. Ohta, N. Suzuki, and Y. Maeda, "Unique fatigue threshold and growth properties of welded joints in a tensile residual stress field," *Int J Fatigue,* vol. 19, pp. 303-310, 1997.

[6]   C. Jang, P.-Y. Cho, M. Kim, S.-J. Oh, and J.-S. Yang, "Effects of microstructure and residual stress on fatigue crack growth of stainless steel narrow gap welds," *Mater Design,* vol. 31, pp. 1862-1870, 2010.

[7]   J. Lanteigne, M. Sabourin, T. Bui-Quoc, and D. Julien, "The characteristics of the steels used in hydraulic turbine runners," presented at the IAHR 24th Symposium on Hydraulic Machinery and Systems, Foz Do Iguassu, Brazil, 2008.

[8]   ASTM, "E647-11e1 Standard Test Method for Measurement of Fatigue Crack Growth Rates," ed: ASTM International, 2011.

[9]   D. Thibault, P. Bocher, and M. Thomas, "Residual stress and microstructure in welds of 13%Cr–4%Ni martensitic stainless steel," *J Mater Process Tech,* vol. 209, pp. 2195-2202, 2009.

[10]   A. G. M. Pukasiewicz, S. L. Henke, and W. J. P. Casas, "Effect of post-weld heat treatment on fatigue crack propagation in welded joints in CA6NM martensite stainless steel," *Welding International,* vol. 20, pp. 947-952, 2006.

[11]   W. Elber, "The significance of fatigue crack closure," *Damage Tolerance in Aircraft Structures, ASTM STP 486,* pp. 230-242, 1971.

[12]   J. C. Newman, "A crack opening stress equation for fatigue crack growth," *Int J Fracture,* vol. 24, pp. 131-135, 1984.

[13]   J. C. Newman Jr, J. H. Crews Jr, C. A. Bigelow, and D. S. Dawicke, "Variations of a global constraint factor in cracked bodies under tension and bending loads," *Constraint Effects in Fracture Theory and Applications: Second Volume, ASTM STP 1244,* pp. 21-42, 1995.

[14]   S. Suresh and R. O. Ritchie, "Near-threshold fatigue crack propagation: a perspective on the role of crack closure," presented at the Symp. on Concepts of Fatigue Crack Growth Threshold, Philadelphia, USA, 1983.

[15]   R. C. McClung, "A literature survey on the stability and significance of residual stresses during fatigue," *Fatigue Fract Eng M,* vol. 30, pp. 173-205, 2007.